Available online at www.sciencedirect.com
ScienceDirect
JOURNAL OF RARE EARTHS, Vol. 29, No. 6, Jun. 2011, P. 516
JOURNAL OF RARE EARTHS
www.re-journal.com/en/

Spectroscopic investigations on the effect of humic acid on the formation and solubility of secondary solid phases of $Ln_2(CO_3)_3$

Stella Antoniou[1], Ioannis Pashalidis[1], Andre Gessner[2], Michael U Kumke[2]

(1. Department of Chemistry, University of Cyprus, P.O. Box 20537, 1678 Nicosia, Cyprus; 2. Chemistry Department/Physical Chemistry, University of Potsdam, Karl-Liebknecht-Str. 24-25, 14476 Potsdam-Golm, Germany)

Received 16 November 2010; revised 6 January 2011

Abstract: The formation of secondary Ln(III) solid phases (e.g., $Nd_2(CO_3)_3$ and $Sm_2(CO_3)_3$) was studied as a function of the humic acid concentration in 0.1 mol/L $NaClO_4$ aqueous solution in the neutral pH range (5–6.5). The solid phases under investigation were prepared by alkaline precipitation under 100% CO_2 atmosphere and characterized by attenuated total reflectance Fourier transform infrared spectroscopy (ATR-FTIR), X-ray diffraction (XRD), time-resolved laser fluorescence spectroscopy (TRLFS), diffuse reflectance ultraviolet-visible (DR-UV-Vis), Raman spectroscopy, and solubility measurements. The spectroscopic data obtained indicated that $Nd_2(CO_3)_3$ and $Sm_2(CO_3)_3$ were stable and remained the solubility limiting solid phases even in the presence of increased humic acid concentration (0.5 g/L) in solution. Upon base addition in the Ln(III)-HA system, decomplexation of the previously formed Ln(III)-humate complexes and precipitation of two distinct phases occurred, the inorganic ($Ln_2(CO_3)_3$) and the organic phase (HA), which was adsorbed on the particle surface of the former. Nevertheless, humic acid affected the particle size of the solid phases. Increasing humic acid concentration resulted in decreasing crystallite size of the $Nd_2(CO_3)_3$ and increasing crystallite size of the $Sm_2(CO_3)_3$ solid phase, and affected inversely the solubility of the solid phases. However, this impact on the solid phase properties was expected to be of minor relevance regarding the chemical behavior and migration of trivalent lanthanides and actinides in the geosphere.

Keywords: lanthanide ions; humic acid; solid phase; solubility; Raman; TRLFS; DR-UV-Vis; rare earths

The long-term performance assessment for the safe disposal of spent fuel in underground geological formations (e.g. clay formations, granite, etc.) requires mechanistic knowledge of the chemical behavior of the radionuclides in aquatic systems, because usually only through underground aquifers, migration and dispersion of the radiotoxic elements in the environment is possible[1]. There is particular interest regarding actinides (e.g., U, Pu, Np, Am Cm), because of the amounts produced in fission reactors and their long-lived radionuclides, which are generally highly radiotoxic alpha radiation emitters. Actinides and lanthanides show similar chemical behavior in solid and aqueous phase, if present in the same oxidation state. This is attributed to the fact that lanthanide elements and particularly Nd and Eu have almost identical ionic radii (112.3 and 108.7 pm, respectively) with actinide elements such as Am and Cm (111.5 and 111 pm, respectively) in the Ln(III) oxidation state[2,3].

The trivalent state is one of the most common oxidation states of minor actinides (e.g., Am and Cm) in aqueous solutions under most environmental conditions. Additionally, the trivalent state is one of the four thermodynamically stable oxidation states of plutonium, which is a key radioelement in spent fuel and maybe the predominant oxidation state under highly reductive conditions[4]. On the other hand, the aquatic chemistry of lanthanide ions is dominated by trivalent oxidation state under environmentally relevant conditions. Because of the direct similarities between the solid and aqueous phase chemistry of some of the actinides and lanthanides and the fact that lanthanides are non-radioactive and possess excellent fluorescent properties, we have used Ln(III) ions as non-radioactive analogues for the An(III) in this study[2].

The chemical behavior of trivalent lanthanide and actinide ions in natural systems is governed by hydrolysis, complexation with naturally occuring ligands, colloid generation, geochemical interaction with mineral surfaces and solid phase formation. The investigation of formed solid phases is of particular interest because secondary phases of trivalent actinides may represent important sinks for minor actinides within nuclear spent fuel repositories and determine their solubility and mobility in the geosphere. Therefore, a mechanistic understanding of the fate and transport mechanisms of minor actinides in natural and contaminated sites requires the investigation of the solubility and relative stability of solid phases formed under natural conditions as key parameters[1]. Although there are several studies regarding solid phase formation and stability[5–8], the number of studies dealing with the impact of naturally occurring matter (NOM)

Foundation item: Project supported by the Cyprus Research Promotion Foundation (ΠΕΝΕΚ/ΕΝΙΣΧ/0308/05 and ΠΡΟΣΒΑΣΗ/ΕΡΥΕΞ/0308/02)

Corresponding author: Ioannis Pashalidis (**E-mail:** pspasch@ucy.ac.cy; **Tel.:** +357-22892785)

DOI: 10.1016/S1002-0721(10)60490-5

on the formation of secondary phases is limited[9,10] and further investigations are needed to understand better the effect of NOM on the solid phase stability and solubility. Investigations on the impact of NOM on solid phase formation and stability are of fundamental importance because NOM (here represented by humic acid) is omnipresent in natural waters and may affect the solution chemistry of metal ions (e.g., complex and colloid formation). Moreover, *in vivo* and *in vitro* studies clearly show that organic matter strongly affects crystal growth as well as texture of minerals and inorganic solids[11,12].

In this study we investigated the effect of humic acid (HA) on the solid phase formation of lanthanide ions in aqueous solutions. The stability of Ln(III) solid phases was studied as a function of the HA concentration in 0.1 mol/L $NaClO_4$ aqueous solutions in the near neutral pH range under normal atmospheric conditions. Characterisation of the solid phases formed in the presence and absence of NOM was performed by TGA, ATR-FTIR, XRD, TRLFS, DR-UV-Vis and Raman spectroscopy. Possible effects of the solid phase alteration on the chemical behavior in aqueous solutions were investigated by solubility measurements in a pH range between 5 and 6.5 using UV-Vis spectrophotometry.

1 Experimental

1.1 Solid phase preparation

Ln(III) stock solutions were prepared by dissolution of $Sm(NO_3)_3{\cdot}6H_2O$ or $Nd(NO_3)_3{\cdot}6H_2O$ (Aldrich Co.) in aqueous 0.1 M $NaClO_4$. $Ln_2(CO_3)_3$ solid phases were prepared by alkaline precipitation (pH 10) of a 50 ml Ln(III) solution under 100% CO_2 atmosphere. The alkaline precipitation took place in pure 0.1 mol/L $NaClO_4$ and 0.1 mol/L $NaClO_4$ solutions containing various amounts of humic acid ([HA]=0.1, 0.3 and 0.5 g/L) under 100% CO_2 atmosphere at 25 °C. According to UV-Vis measurements of the supernatant solutions, HA was quantitatively precipitated with the solid phase yielding samples with different HA contents ($Ln_2(CO_3)_3/x$HA, x=1, 3 or 5 for 0.1, 0.3, and 0.5 g/L HA, respectively). The precipitates, which were magenta for Nd(III) and yellow for Sm(III), corresponding to the different solubility experiments (5<pH<6.5), were separated from the solutions by centrifugation, washed (twice) with de-ionized water, air-dried.

HA solutions used in this study were prepared from Aldrich humic acid, purified and characterized as described elsewhere[13].

1.2 Solid phase characterisation

The precipitates were characterized by thermogravimetric analysis (TGA-50 Shimadzu), and X-ray diffraction (XRD 6000 Shimadzu). FTIR-ATR spectroscopy (IR Prestige-21 Shimadzu) was performed on solid samples after separation by centrifugation.

The evaluation of the particle/crystallite sizes was performed using the Scherrer equation (1).

$$t=\mathrm{k}\cdot\lambda/(B\cdot\cos\theta) \quad (1)$$

In Eq. (1), t is the averaged dimension of crystallites, k the Scherrer constant (assumed to be 0.98), λ the wavelength derived from the XRD measurements, B the FWHM of the most intense reflection, and θ the angle of incidence/reflectance (in radians)[14].

Furthermore, all solid samples were analysed by diffuse reflectance ultraviolet-visible (DR-UV-Vis) spectroscopy (Perkin-Elmer 750). Raman spectra were measured (alpha 300 Raman microscope, WITec) using two different laser wavelengths at l_{Laser}=532 and 785 nm, respectively. The latter laser source was used to minimize fluorescence contributions arising from the organics content present in some of the samples. For the samarium containing samples, a TRLFS analysis was performed at room temperature using a diode pumped Q-switched Nd:YAG-laser/OPO system (Ekspla NT240 series) operating at 1 kHz as excitation light source and an intensified CCD-camera (Andor, DH 734 18H 13) coupled to a spectrograph (Andor Shamrock SR-303i-A) as detection system. The photoluminescence (PL) signal was recorded as time resolved emission spectra (TRES) using the box car technique, providing both, spectral and time-domain information. In a typical experiment the sample was excited at λ_{ex}=464 or 405 nm, the delay after laser pulse was δt=100 ns and the gate width Δt=20 μs. The gate step was adjusted according to the length of the PL decay. The PL decays were analyzed by fitting the integrated PL signal within wavelength intervals corresponding to the different samarium luminescent transitions with an exponential function $f(t)$:

$$f(t)=\sum_{i=1}^{n} A_i \exp(-t/\tau_i)+B \quad (2)$$

where A_i is the amplitude, B the baseline offset (constant) and τ_t the decay time.

1.3 Solubility measurements

For solubility studies the $Ln_2(CO_3)_3$ solid phases (about 100 mg), prepared in the presence and absence of HA, were conducted with 50 ml of 0.1 mol/L $NaClO_4$ solutions under 100% CO_2 atmosphere at 25 ºC. The pH was adjusted by addition of 0.1 mol/L NaOH or 0.1 mol/L $HClO_4$. Following equilibration time (from 2 weeks to one year), pH was measured using a glass electrode (Hanna Instruments pH 211) and the analytical Ln(III) concentration in solution was determined spectrophotometrically (UV 2401 PC Shimadzu) by means of arsenazo-III according to a previously described method[15]. Prior concentration determination, the test solution was ultra-filtrated using 0.45 μm membrane filters to remove any solid phase particulates from the solution. The molar extinction coefficients ε of the Nd(III)-arsenazo and the Sm(III)-arsenazo complex at 650 nm were ε_{Nd}=(197000± 650) L/mol/cm and ε_{Sm}=(114000±650) L/mol/cm, respectively.

2 Results and discussion

According to UV-Vis measurements carried out using the supernatant solutions HA was almost quantitatively (>99%)

co-precipitated with the inorganic solid phase. Hence, it is of particular interest to investigate the effect of HA on the formation and chemical behavior (e.g., solubility) of secondary Ln(III) solids. The investigations regarding possible formation of new Ln(III) solid phases, which may include HA in their structure, the solids were carried out using various spectroscopic methods such as ATR-FTIR, TRLFS, DR-UV-Vis and Raman spectroscopy. Following data obtained from these investigations are presented and discussed.

Fig. 1 shows ATR-FTIR spectra of $Ln_2(CO_3)_3$-5HA solid phases in contact with an aqueous solution of 0.1 M $NaClO_4$. Fig. 1 also includes the ATR-FTIR spectra of the corresponding pure $Ln_2(CO_3)_3$ solid phases. The absence of the narrow band at 3450 cm^{-1}, which corresponds to the coordinated hydroxo group is not observed in the FTIR-ATR spectrum of the solid and confirms the formation of pure $Ln_2(CO_3)_3$ solid phases. The absorption bands around 1375 cm^{-1} correspond to the symmetric and anti-symmetric stretching of the complexed carbonates respectively. The absence of any new peaks in the spectra related to HA indicates that only $Ln_2(CO_3)_3$ solids are formed and most probably HA is just physically adsorbed on the inorganic particles.

Complementary to the ATR-FTIR spectroscopy, the $Ln_2(CO_3)_3$ solids were investigated also by Raman spectroscopy. Raman spectra of $Ln_2(CO_3)_3$ solids prepared in the absence and presence of humic acid are shown in Fig. 2 (λ_{Laser}=532 nm). The spectra of the pure $Ln_2(CO_3)_3$ solids showed the characteristic ligand (carbonate) bands at 1065 cm^{-1} [16], proving the formation of the $Ln_2(CO_3)_3$ solid phases. The Raman spectra of the $Ln_2(CO_3)_3$/xHA are strongly affected by the intrinsic fluorescence of the humic acid chromophores, which extensively overlaps the Raman bands of the $Ln_2(CO_3)_3$ solids. In order to minimize the impact of the

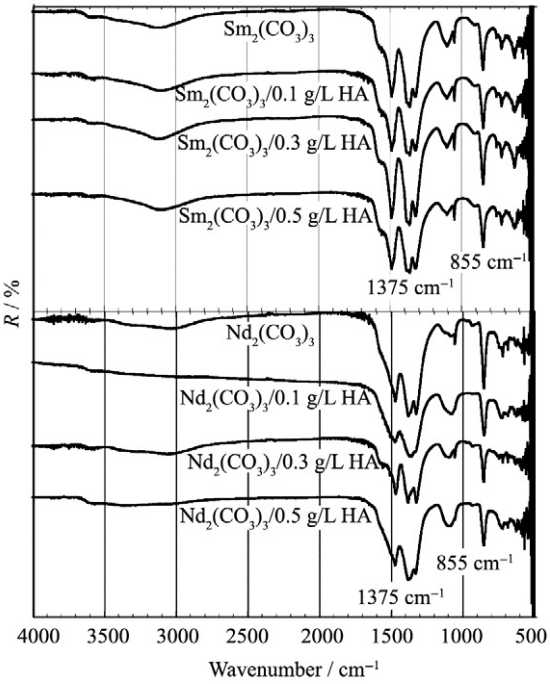

Fig. 1 ATR-FTIR spectra of the $Ln_2(CO_3)_3$ solid phases prepared in presence and absence of HA

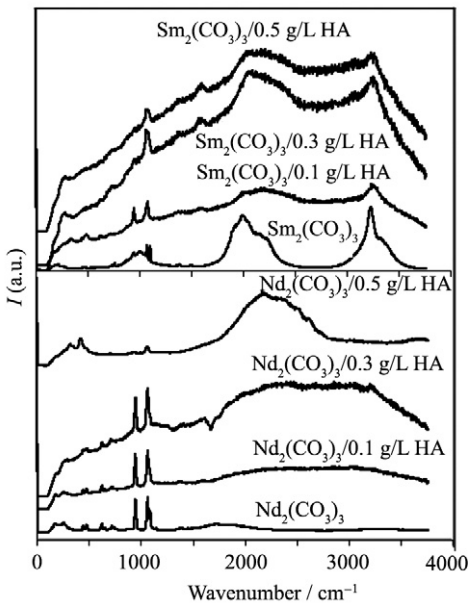

Fig. 2 Raman spectra of the $Ln_2(CO_3)_3$ solid phases prepared in presence and absence of HA, using a laser source at 532 nm

humic acid fluorescence, another set of Raman spectra was obtained at λ_{Laser}=785 nm. Excitation at 785 nm results in significantly lower fluorescence of the HA because of the much lower absorption probability of the HA chromophores at this wavelength. The corresponding spectra are shown in Fig. 3, which in contrast to Fig. 2 shows only an enlarged section of the spectrum from 0–1500 cm^{-1}.

Comparing the Raman spectra collected for $Ln_2(CO_3)_3$ at 532 and 785 nm excitation, it is found that for Sm(III) both spectra are identical as expected. However, in case of Nd(III) the spectral intensity distribution was strongly dependent on the laser wavelength. The Raman spectra measured with λ_{Laser}=785 nm show very strong, but broad Raman bands around 1265 cm^{-1}. The observed enhancement may be attributed to a resonance Raman effect induced by exciting

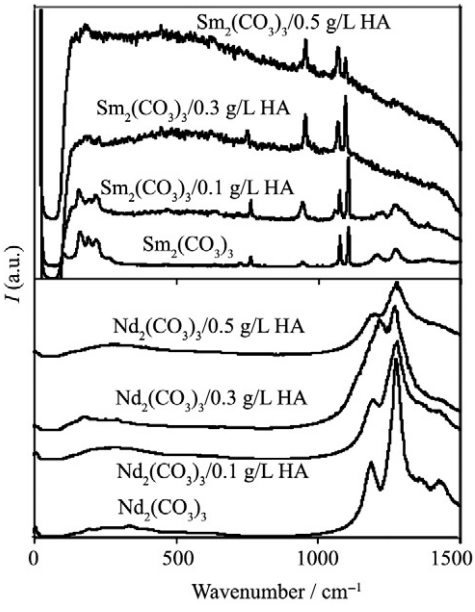

Fig. 3 Raman spectra of the $Ln_2(CO_3)_3$ solid phases prepared in presence and absence of HA, using a laser source at 785 nm

close to an absorption band of Nd(III). The comparison of this Raman band for $Nd_2(CO_3)_3$ and $Nd_2(CO_3)_3$/5HA shows a slight peak broadening in the presence of HA, which may be attributed to slight changes in the solid phases or to additional HA related Raman bands, which can also be found in this spectral region[17].

The occurrence of a resonance Raman effect at λ_{Laser}=785 nm for the $Nd_2(CO_3)_3$ solid phase is corroborated by the diffuse DR-UV-Visible spectra (see Fig. 4), which show a strong absorbance band at 785 nm. In contrast to $Nd_2(CO_3)_3$, $Sm_2(CO_3)_3$ does not show any absorption band at this wavelength.

The Raman spectra obtained by means of the 785 nm source show that there is no difference between $Ln_2(CO_3)_3$ and $Ln_2(CO_3)_3$/*x*HA solids, indicating that under normal atmospheric conditions and even in the presence of increased HA (natural organic matter) concentration, $Ln_2(CO_3)_3$ remains the sole solubility limiting solid phase. This is also supported by the DR-UV-Vis measurements. Like the Raman spectra the DR-UV-Vis spectra are similar for $Ln_2(CO_3)_3$ and $Ln_2(CO_3)_3$/*x*HA solids, indicating that the HA does not affect the composition and structure of the Ln(III) solids. The formation of two distinct phases, the inorganic ($Ln_2(CO_3)_3$) and the organic phase (HA) is of particular interest taking into account the relative high affinity of HA for trivalent lanthanides in solution[18].

Additionally, the $Sm_2(CO_3)_3$ solids were investigated by TRLFS spectroscopy. The emission spectra (Fig. 5) show four emission peaks centered at 564, 601, 650 and 708 nm corresponding to the $^4G_{5/2}\rightarrow{}^6H_J$ transitions, with J=5/2, 7/2, 9/2 and 11/2, respectively. A small change in the intensity ratio between the $^4G_{5/2}\rightarrow{}^6H_{7/2}$ and the $^4G_{5/2}\rightarrow{}^6H_{9/2}$, $^6H_{11/2}$ transitions was observed with increasing HA concentration (see Fig. 5). The fluorescence decays for all samples were monoexponential. The decay times for all Sm(III) samples are very similar (946 ns<τ<1011 ns) and no systematic influence of the HA on the solid phase composition could be

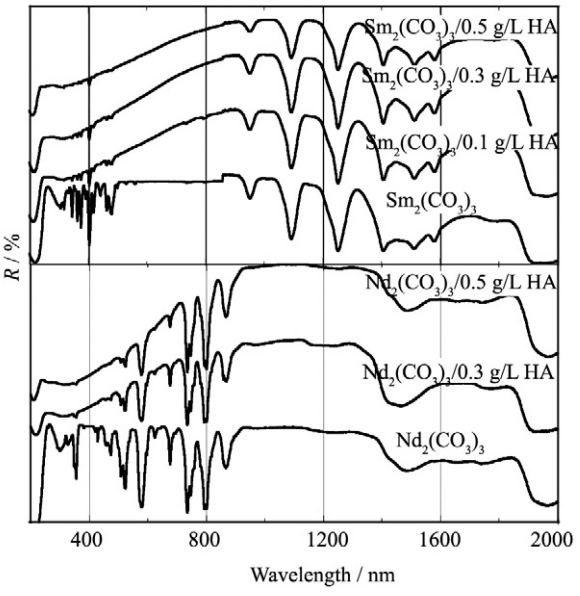

Fig. 4 DR-UV-Vis spectra of the $Ln_2(CO_3)_3$ solid phases prepared in presence and absence of HA

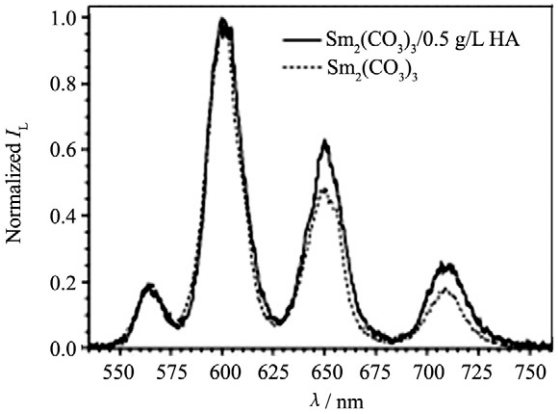

Fig. 5 Emission spectra of $Sm_2(CO_3)_3$ (dashed line) and $Sm_2(CO_3)_3$ with 0.5 g/L HA (solid line) at δt=100 ns, λ_{ex}= 464 nm

observed (see Table 1). Compared to the Sm(III) decay time in water (2.3 μs<τ_{H_2O}<2.7 μs)[19,20] or in other solids such as Sm(III) doped glasses, oxides or even organic complexes (500 μs<τ<3.1 ms)[21–27] the decay times determined for the $Sm_2(CO_3)_3$ and $Sm_2(CO_3)_3$-*x*HA solids are distinctly shorter. This may be explained by fast (phonon-assisted) relaxation pathways provided by the coordinating CO_3^{2-} ions in the solids.

Generally, the spectroscopic investigation are in agreement and indicated clearly that precipitation of the $Ln_2(CO_3)_3$ solids (even in the presence of increased HA concentration) resulted in the formation of the pure solids. Formation of solids containing in their structure HA was not observed and the HA co-precipitated with the inorganic solid was just physically adsorbed on the surface of the $Ln_2(CO_3)_3$ particles. The separation into an inorganic and an organic phase during precipitation was somehow unexpected, taking into account the relatively high affinity of HA for the Ln(III) ions resulting in stable Ln(III)-humate complexes in solution[18]. The formation constants of the Ln(III)-humate complexes (lgβ~7) were relatively larger than the corresponding formation constants for carbonate complexation (lgβ1~5)[28]. However, in the alkaline pH range (pH 10), where the solid phase formation occurred, the concentration of the carbonate ligand became predominant resulting in the decomplexation of the Ln(III)-humate complex and the formation of the $Ln_2(CO_3)_3$ solids.

In order to validate the spectroscopic data and investigate possible effects of the adsorbed HA on the solid phase texture (e.g. particle size), XRD measurements were performed. Fig. 6 shows the XRD diffractograms of $Ln_2(CO_3)_3$ and $Ln_2(CO_3)_3$/*x*HA solids. In agreement with the spectro-

Table 1 Fluorescence decay time τ of the $Sm_2(CO_3)_3$ solid phase prepared in the absence and presence of different amounts of humic acid in solution (The average error in τ is ± 5 ns.)

Samples	τ (ns) at 464 nm
$Sm_2(CO_3)_3$	946
$Sm_2(CO_3)_3$/0.1 g/L HA	1013
$Sm_2(CO_3)_3$/0.3 g/L HA	1019
$Sm_2(CO_3)_3$/0.5 g/L HA	1011

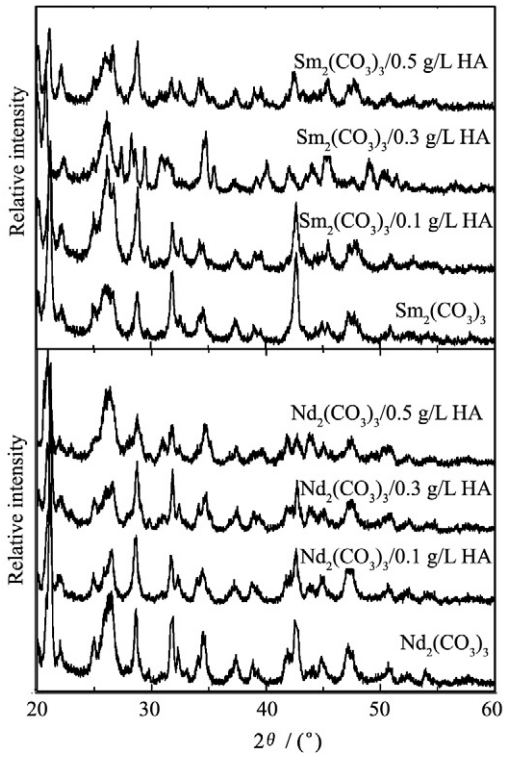

Fig. 6 XRD diffractograms of the $Ln_2(CO_3)_3$ solid phases prepared in presence and absence of HA

scopic data, the XRD spectra indicate only the presence of $Ln_2(CO_3)_3$. Identification of the compound formed was made by comparison of d-spacings with the corresponding JCPDS card ($Ln_2(CO_3)_3 \cdot 8H_2O$, 31-877) and literature data[29]. The particle/crystallite sizes were calculated according to Eq. (1) and are summarized in Table 2.

The data show that HA affects differently the particle/crystallite size of the $Nd_2(CO_3)_3$ and the $Sm_2(CO_3)_3$ solid phases. The crystallite size of $Nd_2(CO_3)_3$ solid decreases, whereas the crystallite size of $Sm_2(CO_3)_3$ solid increases with increasing humic acid concentration in solution. The opposite effect of HA on the particle size of the two different lanthanide solid phases can be attributed to the different ionic radii of the corresponding elements[2,28]. Moreover, the changes in particle size may affect accordingly the solid phase solubility because of microsolubility effects[30].

Possible microsolubility effects were investigated by solubility experiments using two different $Ln_2(CO_3)_3$ solids, prepared in absence and presence of HA and the corresponding data are graphically shown in Fig. 7. According to the solubility data (Fig. 7), microsolubility effects (even small) are apparent, resulting (as expected) in lower solubility (about 0.5 log-units) for $Sm_2(CO_3)_3/x$HA and slightly higher solubility (about 0.5 log-units) for $Nd_2(CO_3)_3/x$HA in comparison to the corresponding pure solids. However, these changes in the solubility of the solids are within the uncertainty found in literature regarding the values of solubility product ($-31.4 < \lg K_{sp} < -34.4$)[32,33].

Table 2 Particle size (nm) of the $Nd_2(CO_3)_3$ and $Sm_2(CO_3)_3$ solid phases precipitated in aqueous solutions of 0.1 mol/L $NaClO_4$ containing various amounts of humic acid (The particle size was estimated from the XRD spectra/peaks according to Scherrer equation[31].)

[HA]/(mg/L)	$Nd_2(CO_3)_3$	$Sm_2(CO_3)_3$
0	36.8 ± 0.5	21.8 ± 0.5
0.1	17.9 ± 0.5	24.2 ± 0.5
0.3	14.4 ± 0.5	27.5 ± 0.5
0.5	14.2 ± 0.5	54.5 ± 0.5

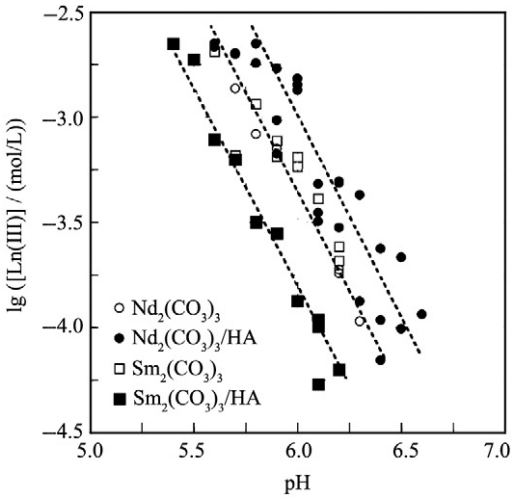

Fig. 7 Solubility curves of the $Ln_2(CO_3)_3$ solid phases prepared in presence and absence of HA

3 Conclusions

The formation of secondary solid phases of lanthanides (e.g. $Ln_2(CO_3)_3$) was not significantly affected by the presence of humic acids in an aqueous system. The spectroscopic data obtained by FTIR, Raman, TRLFS, DR-UV-Vis spectroscopy clearly showed that only the pure $Ln_2(CO_3)_3$ solid was formed and the HA was just co-precipitated, most probably adsorbed onto the solid particles.

However, the adsorption of humic acids on the particle surface affected the texture of the solid phase formed, resulting in different particle sizes (as indicated by XRD measurements) and different water holding capacity of the solid phase (as indicated by TGA measurements) in the presence of HA.

The changes in the solid phase solubility because of microsolubility effects were relatively small and within the uncertainties of the solubility product values given in literature[31,32] for $Ln_2(CO_3)_3$ solid phases.

The impact of humic acids on the chemical behavior and migration of trivalent lanthanides and actinides in the geosphere because of their impact in the formation of secondary solid phases was expected to be of minor relevance and significantly lower than their impact because of the formation of HA complexes with the lanthanide and actinide ions. However, coating of nano-sized solid phase particles with HA colloids could increase their stability in the aqueous phase and resulted in enhanced contaminant mobility in the

geo- and biosphere[34]. Since colloidal transport played an important role in contaminant/radionuclide transport, the formation of HA-coated inorganic particles could be subject of further investigation.

References:

[1] Kim J I. Significance of actinide chemistry for the long-term safety of waste disposal. *Nucl. Eng. Technol.*, 2006, **38**: 459.

[2] Seaborg G T. Overview of the actinide and lanthanide (the f) elements. *Radiochim. Acta*, 1993, **61**: 115.

[3] Gregory R C. Comparative solution chemistry of the 4f and 5f elements. *J. Alloys Compd*., 1995, **223**: 174.

[4] Choppin G R. Actinide speciation in the environment. *J. Radioanal. Nucl. Chem.*, 2007, **273**: 695.

[5] Pashalidis I, Runde W, Kim J I. A study of solid-liquid phase equilibria of Pu(VI) and U(VI) in aqueous carbonate systems. *Radiochim. Acta*, 1993, **61**: 141.

[6] Meinrath G, Kato Y, Kimura T, Yoshida Z. Solid-aqueous phase equilibria of uranium under ambient conditions. *Radiochim. Acta*, 1996, **75**: 159.

[7] Craig F, Robert E, Jack P, Eugene K. A study on the effects of drying conditions on the stability of $NaNd(CO_3)_2{\cdot}6H_2O$ and $NaEu(CO_3)_2{\cdot}6H_2O$. *Appl. Geochem.*, 2002, **17**: 1305.

[8] Runde W, Van Pelt C, Allen P G. Spectroscopic characterization of trivalent f-element (Eu, Am) solid carbonates. *J. Alloys Compd.*, 2000, **303-304**: 182.

[9] Kolokassidou C, Pashalidis I. Effect of humic acid on the solid phase stability and solubility of $UO_2(OH)_2$. *J. Radioanal. Nucl. Chem.*, 2099, **279**: 523.

[10] Antoniou S, Kolokassidou C, Polychronopoulou K, Pashalidis I. Effect of humic acid on the solid phase stability of UO_2CO_3. *J. Radioanal. Nucl. Chem.*, 2009, **279**: 863.

[11] Kitano Y, Kanamori N, Tokuyama A. Effects of organic matter on solubilities and crystal forms of carbonates. *Am. Zool*., 1969, **9**: 681.

[12] Kodona E K, Alexopoulos C, Panou E, Pomonis P J. Self-organized meso- and hybridic phases of poly(aspartic acid) and poly(glutamic amino acid) with cationic surfactants (C_nTAB, n=14, 16) and a silica source (TEOS). *Chem. Mater.*, 2007, **19**(7): 1853.

[13] Kolokassidou K, Szymczak W, Wolf M, Obermeier C, Buckau G, Pashalidis I. Hydrophilic olive cake extracts: Characterization by physicochemical properties and Cu(II) complexation. *J. Hazard. Mater.*, 2009, **164**: 442.

[14] Wang Y Q, Yu X J, Sun D Z. Synthesis, characterization, and photocatalytic activity of $TiO_{2-x}N_x$ nanocatalyst. *J. Hazard. Mater.*, 2007, **144**: 328.

[15] Lu Y W, Laurent G, Pereira H. A novel methodology for evaluation of formation constants of complexes: example of lanthanide-arsenazo III complexes. *Talanta*, 2004, **62**: 959.

[16] Rutt H N, Nicola J H. Raman spectra of carbonates of calcite structure. *J. Phys. C: Solid State Phys.*, 1974, **7**: 4522.

[17] Corrado G, Sanchez-Cortes S, Francioso O, Garcia-Ramos J V. Surface-enhanced Raman and fluorescence joint analysis of soil humic acids. *Anal. Chim. Acta*, 2008, **616**: 69.

[18] Konstantinou M, Kolokassidou K, Pashalidis I. Studies on the interaction of olive cake and its hydrophylic extracts with polyvalent metal ions (Cu(II), Eu(III)) in aqueous solutions. *J. Hazard. Mater.*, 2009, **166**: 1169.

[19] Takaumi K, Yoshiharu K. Luminescence study on determination of the hydration number of Sm(III) and Dy(III). *J. Alloys Compd.*, 1995, **225**: 284.

[20] Gregory R C, Dean R P. Applications of lanthanide luminescence spectroscopy to solution studies of coordination chemistry. *Coord. Chem. Rev.*, 1998, **174**: 283.

[21] Grażyna D D. Sm^{3+}-doped $LiNbO_3$ crystal, optical properties and emission cross-sections. *J. Alloys Compd.*, 2005, **391**: 26.

[22] Li Z F, Yu J B, Zhou L, Zhang H J, Deng R P. The optical properties and the natural lifetime calculation of a Sm(III) complex. *Inorg. Chem. Comm.*, 2008, **11**: 1284.

[23] Saleem S A, Jamalaiah B C, Kiwan J, Jayasimhadri M, Mohan B A, Suresh K J, Rama M L. Sm^{3+} luminescence in alkali lead tellurofluoroborate glasses. *IOP Conf. Ser.: Mater. Sci. Eng.*, 2009, **2**: 012049.

[24] Marcin S, Przemysław S, Radosław L, Witold R R. Synthesis, optical spectra and radiative properties of Sm_2O_3:PbO:P_2O_5 glass materials. *Opt. Mater.*, 2008, **30**: 1571.

[25] Bunzli, J-C G, Eliseeva, S V. Lanthanide NIR luminescence for telecommunications, bioanalyses and solar energy conversion. *J. Rare Earths*, 2010, **28**: 824.

[26] Li H, Xian H, Zhao G. Synthesis and crystal structures of La(III), Y(III) complexes of homoveratric acid with 1,10-phenanthroline. *J. Rare Earths*, 2010, **28**: 7.

[27] Chen X Y, Luo W Q, Liu Y S, Liu G K. Recent progress on spectroscopy of lanthanide ions incorporated in semiconductor nanocrystals. *J. Rare Earths*, 2007, **25**(5): 515.

[28] Kim J I. The chemical behavior of transuranium elements and barrier functions in natural aquifer systems. *Mater. Res. Soc. Symp. Proc.*, 1993, **294**: 3.

[29] Hinode H, Sharma R, Eyringa L. Study of the decomposition of neodymium Hydroxy carbonate and neodymium carbonate hydrate. *J. Solid State Chem*., 1990, **84**: 102.

[30] Kellner R, Mermet J M, Otto M, Widmer H M. Analytical Chemistry. Weinheim: Wiley-VCH, 1998.

[31] Jenkins R, Snyder R L. Introduction to X-ray Powder Diffractometry. Now York: John Wiley & Sons Inc., 1996.

[32] Runde W, Meinrath G, Kim J I. A study of solid-liquid phase equilibria of trivalent lathanide and actinide ions in carbonate systems. *Radiochim. Acta*, 1992, **58/59**: 93.

[33] Firsching F H, Mohammadzadel J. Solubility products of the rare-earth carbonates. *J. Chem. Eng. Data*, 1986, **31**: 40.

[34] Liang T, Ding S M, Song W C, Chong Z Y, Zhang C S, Li H T. A review of fractionations of rare earth elements in plants. *J. Rare Earths*, 2008, **26**: 7.